PCCP

Accepted Manuscript


This is an *Accepted Manuscript*, which has been through the Royal Society of Chemistry peer review process and has been accepted for publication.

*Accepted Manuscripts* are published online shortly after acceptance, before technical editing, formatting and proof reading. Using this free service, authors can make their results available to the community, in citable form, before we publish the edited article. We will replace this *Accepted Manuscript* with the edited and formatted *Advance Article* as soon as it is available.

You can find more information about *Accepted Manuscripts* in the Information for Authors.

Please note that technical editing may introduce minor changes to the text and/or graphics, which may alter content. The journal's standard Terms & Conditions and the Ethical guidelines still apply. In no event shall the Royal Society of Chemistry be held responsible for any errors or omissions in this *Accepted Manuscript* or any consequences arising from the use of any information it contains.

ROYAL SOCIETY OF CHEMISTRY

www.rsc.org/pccp

Journal Name

ARTICLE

# Interfacial zippering-up of coiled-coil protein filaments

Emiliana De Santis,[a] Valeria Castelletto[a] and Maxim G. Ryadnov[a]*

Received 00th January 20xx,
Accepted 00th January 20xx

DOI: 10.1039/x0xx00000x

www.rsc.org/

Protein self-assembled materias find increasing use in medicine and nanotechnology. A challenge remains in our ability to tailor such materials at a given length scale. Here we report a de novo self-assembly topology which enables the engineering of filamentous protein nanostructures under morphological control. The rationale is exemplified by a ubiquitous self-assembly motif – an α-helical coiled-coil stagger. The stagger incorporates regularly spaced interfacial tryptophans which allows it to zipper up into discrete filaments that bundle together without thickening by maturation. Using a combination of spectroscopy, microscopy, X-ray small-angle scattering and fibre diffraction methods we show that the precise positioning of tryptophan residues at the primary and secondary structure levels defines the extent of coiled-coil packing in resultant filaments. Applicable to other self-assembling systems, the rationale holds promise for the construction of advanced protein-based architectures and materials.

## Introduction

An emerging tendency across different industry sectors is a pursuit for physico-chemical systems with a better control over material form and structure.[1] Self-assembling biomolecular structures hold a particular promise in this regard.[2] These cover a much broader chemical space, when compared to other molecular classes, and uniquely exploit synergies between covalent and non-covalent arrangements that enable hierarchically complex materials.[3] Peptide self-assembling systems offer perhaps the richest repertoire of different material forms when compared to other molecular cases.[2] Indeed, they find use in applications as different and unrelated as gene therapy and molecular electronics or regenerative medicine and environmental monitoring.[4,5]. However, challenges remain in finding exploitable relationships between peptide sequences and the morphologies of resultant materials, which ultimately defines the choice of predictable assembly patterns.[2] One of such patterns is encoded by an α-helical coiled-coil stagger.[6] This is a ubiquitous motif for peptide assembly exemplified by the natural and synthetic designs of predominantly filamentous origin.[6-8] The motif is a super-helix or bundle of two to five α-helices whose sequences use a heptad repeat pattern of hydrophobic (*H*) and polar (*P*) amino-acid residues (*PHPPHPP*). Such a pattern is normally designated *gabcdef*, in which *a* and *d* form hydrophobic interfaces that determine the number of helices in the bundle, while *g* and *e* of successive heptads (*g*-*e*′ pairs) provide complementary charges that produce an axial stagger of the helices.[9] The periphery and solvent-exposed *b*, *c* and *f* sites are not directly involved in the assembly, but can impact on the fiber morphology showing direct correlations with peptide sequences and lengths.[10] This suggests that the motif provides a structurally permissive supramolecular background and can incorporate properties that are not typical of naturally occurring counterparts, but may be characteristic of other assembly motifs. This reasoning brings an opportunity of creating hybrid materials by applying properties of one assembly type to advance another.[11] An outstanding characteristic here is the use of aromatic residues in very short peptides which assemble into β-pleated structures.[4] Yet, coiled-coil staggers are longer sequences that assemble longitudinally. This, on the one hand, allows β-sheets to be exclusively built of aromatic residues held together via π-π stacking interactions, which normally culminates in gelation;[3] and, on the other hand, enables α-helical sequences to incorporate the residues at regular but long intervals to disfavour gelation and favour the assembly of discrete filaments. Granted successful such an approach would provide a major determinant of fibre morphology which is proving critical for applications that rely on the dimensional aspects of nanomaterials.[1-3]

## Results and Discussion

### Design

To probe this, we built upon the previously described self-assembly templates[10] that furnish uniform fibres with mean diameters of 4-8 nm corresponding to 2-4 coiled-coil filaments per fibre. More specifically, we designed an experimental model comprising three cationic and three anionic heptads, with two tryptophan residues symmetrically incorporated into

[a]National Physical Laboratory, Hampton Rd, Teddington, Middlesex, TW11 0LW, UK. * E-mail: max.ryadnov@npl.co.uk

† Footnotes relating to the title and/or authors should appear here.

Electronic Supplementary Information (ESI) available: [details of any supplementary information available should be included here]. See DOI: 10.1039/x0xx00000x

This journal is © The Royal Society of Chemistry 20xx



Please do not adjust margins

Physical Chemistry Chemical Physics Accepted Manuscript

the *f* sites of the N- and C-terminal heptads and one in the central heptad (**Table 1** and **Figure 1**). The choice of tryptophan residues was inspired by tryptophan zippers (β and α) in which tryptophans enable hydrophobic interfaces via tight cross-strand packing in β-sheets[12] and knobs-into-holes packing in coiled-coils.[13] In contrast, in our model, tryptophans are placed in the solvent-exposed face of each helix with a maximum exposure and away from the *a*-*d* coiled-coil interface. The number of tryptophans used in the sequence is low to compromise the solvation of the coiled-coil bundle, but sufficient to enable moderate attractions between different bundles. Such interactions can only be realized through direct contacts between tryptophan residues, which are likely to involve π-π stacking. To provide a sufficiently large surface area for these to occur, leucine residues that have preference for trimeric bundles were chosen to form the hydrophobic interface.[14-16] Lysines and glutamates were used in cationic and anionic heptads, respectively, to enable *g*-*e*′ pairs, whereas small alanines and neutral polar glutamines that help to minimize lateral associations of coiled-coil oligomers occupied the remaining solvent exposed sites (Table 1 and Figure 1).[9] All the residues, with the obvious exception of tryptophans, have high helical propensities. The peptide was uncapped to facilitate electrostatic interactions between its abutting termini thereby supporting the longitudinal propagation of the staggered coiled coils (Figure 1).[17]

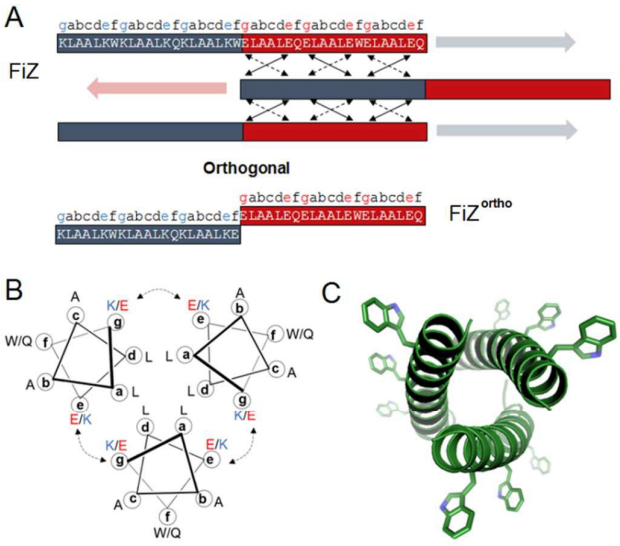


**Figure 1**. Peptide design. (A) The filamentous zipper, FiZ, peptide (upper) and its orthogonal version FiZ$^{ortho}$ (below), comprising cationic (blue) and anionic (red) coiled-coil domains arranged into a trimeric stagger. Double arrows indicate *g*-*e*′ electrostatic interactions, with one of the two combinations, bold or dashed arrows, preferred within one coiled coil. (B) Coiled-coil helical-wheels of the trimer with double arrows indicating electrostatic interactions. (C) Top view of a coiled-coil model trimer (PDB entry 1IJ3 rendered by PyMOL) highlighting interfacial tryptophan residues (not to scale).

Upon folding hydrophobic coiled-coil interfaces favour the persistent longitudinal elongation of the formed staggers by loosening electrostatic interactions and freeing up some *g* and *e* sites. At any given time, any *g*-*e*′ pair of one helical pair in the trimer can be replaced by a mirror *g*-*e*′ pair of another helical pair. Unengaged *g*-*e*′ pairs make fibre surfaces highly polar and charged which disfavours fibre thickening. All pair re-engagements are concomitant along the aligned sequences to render changes in the entire electrostatic network highly cooperative.[14] The model allows to fine-tune inter-stagger interactions owing to tryptophan residues being regularly spaced at the super-helix pitch distances (1.63 nm)[18] thus promoting the zippering up of coiled coils into discrete filaments which then may bundle up without thickening by maturation. To reflect on this rationale, the peptide was termed a filamentous zipper (FiZ) and was accompanied with three control peptides (Table 1). One was identical to FiZ, with all *f* sites made phenylalanines. This peptide, dubbed FiF, was also expected to assemble into coiled coils. However, phenylalanines introduced in each heptad make up more extended hydrophobic interfaces that are meant to disrupt super-helix alignments compromising extended inter-filament associations.[19] Two other controls were made as orthogonally linked cationic and anionic FiZ domains.[9] An orthogonal version (FiZ$^{ortho}$) was to physically separate the two domains and disrupt the continuity of the super-helix pitch thus constraining extensive filament bundling.[17] The final control has no aromatic residues and was meant to break the assembly, hence dubbed a filament breaker, FiB$^{ortho}$ (Table 1).[17]

**Table 1.** Peptide sequences used in the study

| Name | Sequence[a] | | | | | |
|---|---|---|---|---|---|---|
| | gabcdef | gabcdef | gabcdef | gabcdef | gabcdef | gabcdef |
| T2[b] | KIAALKQ | KIAALKK | ..... | EIAALEY | EIAALEQ | ..... |
| FiZ | KLAALK**W** | KLAALKQ | KLAALK**W** | ELAALEQ | ELAALE**W** | ELAALEQ |
| FiF | KLAALK**F** | KLAALK**F** | KLAALK**F** | ELAALE**F** | ELAALE**F** | ELAALE**F** |
| FiZ$^{ortho}$ | KLAALK**W** | KLAALKQ | KLAALK**X** | ELAALEQ | ELAALE**W** | ELAALEQ |
| FiB$^{ortho}$ | KLAALKQ | KLAALKQ | KLAALK**X** | ELAALEQ | ELAALEQ | ELAALEQ |

[a]X is a glutamate forming an isopeptide (orthogonal) bond with the first glutamate of the anionic domain. The Cα carboxyl is uncapped and charged; [b] use of original nomenclature.[10]

## Folding and assembly

Consistent with the design, circular dichroism (CD) spectroscopy revealed appreciable α-helical signals (>50%)[20] for all the peptides at micromolar chain concentrations (**Figure 2a**).

The dampening of the signal at 208 and a red-shifted minimum centred at 226 nm were apparent for FiZ and FiF. These spectral features are common for particulate self-assembled systems and may be accompanied by increases in turbidity and solution clouding,[6,17] signs of which were observed for the peptides at elevated temperatures. Importantly, signal decreases at 208 nm can be a function of super-helix tilt angles for one aromatic ring per superhelix,[21] while the superposition of induced aromatic bands can equally contribute to the red shift suggesting that tryptophan and phenylalanine residues

Physical Chemistry Chemical Physics Accepted Manuscript



This journal is © The Royal Society of Chemistry 20xx

Please do not adjust margins

may be in a constrained chiral environment.[22] Small angle X-ray scattering (SAXS) performed under the same conditions supported the conjecture and revealed the formation of discrete filaments for FiZ (Figure 2B). The fitting of SAXS curves to the form factor of a long cylinder[23] returned a radius of 7.3 ± 3 nm indicative of filamentous assembly. In contrast, improved fitting in the low q range[24] for FiF gave a smaller radius of 3±1 nm exposing the lack of fibre formation (Figure 2B, Table S1).

Consistent with this, transmission electron microscopy (TEM) revealed relatively uniform and individually discrete filaments of 3.4 ± 0.8 nm in diameter were evident for FiZ. The filaments tended to associate into larger bundles, which is atypical for fibre thickening characterized by maturation (**Figure 3A**).[8] No apparent fibrillogenesis was observed for FiF. Nonetheless, similar CD signals and clear-cut radii by SAXS for FiZ and FiF imply that both assemble in a cooperative manner. Indeed, CD spectra recorded during thermal unfolding of the peptide gave clear isodichroic points at 202 nm (Figure S1 in Supporting Information). The signal intensity at this wavelength remained the same and is indicative of a two-state transition between helical and unfolded forms (Figure S1).

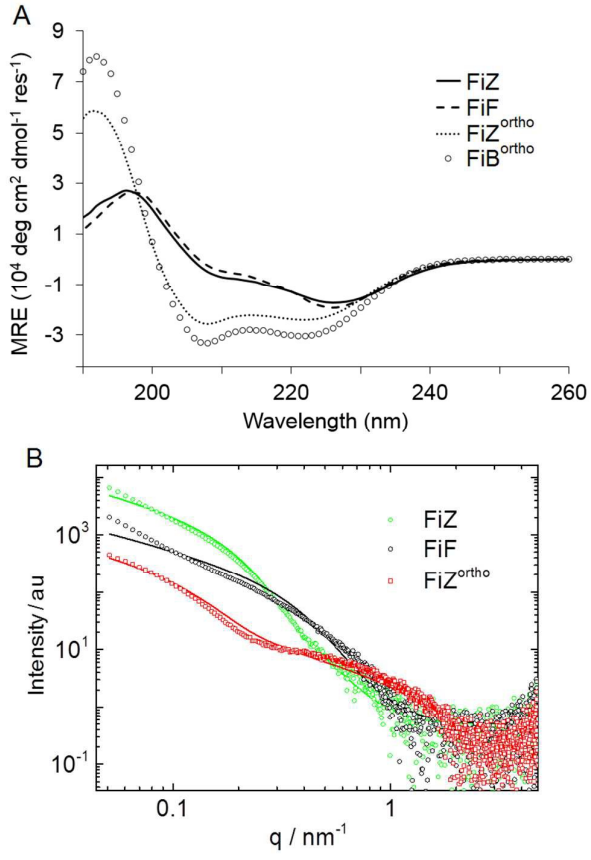


**Figure 2**. Peptide folding. (A) CD spectra for FiZ (solid line), FiF (dashed line), FiZortho (dotted line) and FiBortho (open circles). (B) SAXS curves for FiZ (green), FiF (black) and FiZortho (red) fitted according to a system of long cylinders. Folding conditions: peptide at 100 µM in 10 mM MOPS, pH 7.4, room temperature.

Thermal denaturation curves were approximately linear, which points to multiple helical conformers, due to the concomitant electrostatic networks, and partial helix fraying, due to the structuring of the aromatic residues (Figure S1). For both peptides aromatic residues appeared to be conformationally locked suggesting extended coiled-coil assembly. However, only FiZ formed persistent filamentous structures (Figure 3A).

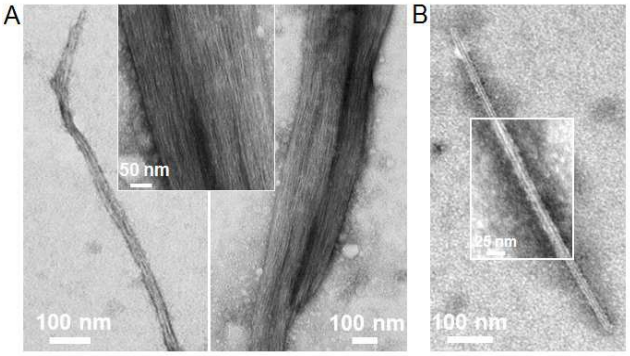


**Figure 3.** Peptide assembly. Transmission electron micrographs for FiZ (A) and FiZ$^{ortho}$ (B). Assembly conditions: peptide at 100 µM in 10 mM MOPS, pH 7.4, room temperature.

**Structural analysis**

To gain a detailed insight into how the ultrastructure of all four designs may relate to the differences observed by spectroscopy and microscopy, X-ray diffractions (XRD) from the oriented and partly dried assemblies of the peptides were attempted (Figures 4 and S2). XRD patterns for FiZ and FiF peptides contained clear d-spacings around 9.5 and 4.3 Å (4.7 Å for FiF). The peak centred at 4.3 Å bears a relationship to intra-helical distances reported for discrete coiled-coil assemblies.[25] The peak is too broad and diffuse to correspond to the typical β-sheet spacing of 4.7 Å, which, together with no apparent signs of β-structure by Fourier transform infra-red (FT-IR) spectroscopy (Figure S3) and the predominantly α-helical CD spectra (Figures 2A, S1), indicate that assemblies are helical. Complementary to this, the spacing at 9.5 Å matches perfectly an average distance between helical axes in coiled-coils.[25] A spacing at 17.1 Å observed for FiZ, reflects averaged packing distances between coiled coils in the filaments. For typical coiled-coil fibres these distances are 18.2 Å.[6] However, closer packing (17.3 Å) was reported for tighter interfaces between coiled coils,[26] which in FiZ are expected to occur at the expense of tryptophan zippering. The same spacing could not be assigned for FiF confirming that FiF coiled coils did not pack.

Combined the data prompts a differential mode for the FiZ/FiF assembly: (i) both FiZ and FiF staggers propagate into extended coiled coils, but (ii) only FiZ coiled coils interlock into discrete filaments that bundle up. Such a mode of assembly does not assume specific packing of coiled coils but is different from a geometrically rigid hexagonal packing of double-stranded coiled coils reported for filamentous assemblies without interfacial aromatic interactions.[6,26]

Physical Chemistry Chemical Physics Accepted Manuscript

To probe this under the same assembly conditions, an XRD pattern was obtained for our recently reported T2 design[10] (Table 1). The peptide comprises four heptads and is based on a similar sequence template. It folds into double-stranded coiled coils with pronounced solvated surfaces (glutamine and lysine residues in f sites) preventing extended lateral associations, and assembles into 6-nm-wide filaments,[10] consistent with the hexagonal packing of coiled-coil fibers.[6] A spacing at 41.6 Å obtained for T2 closely matches the repeat distance of 28 residues in a fully folded α-helical coiled-coil.[6] Equatorial arcs with d-spacings at 22.9, 15.9, 10.6 and 8.2 Å ($d_{100}$, $d_{110}$, $d_{200}$ and $d_{210}$) reflect the coiled-coil packing in the lateral plane (*ab*), perpendicular to the coiled-coil axes. The signals index on a hexagonal lattice with coiled-coils being 26.4 Å apart (Figure S4). This increased distance, from a more common 18.2 Å, can be accounted for three molecules of interfacial water (2.7 Å), which is expected for hydrophilic and charged coiled-coil surfaces and correlates well with the tighter packing in FiZ (17.3 Å).

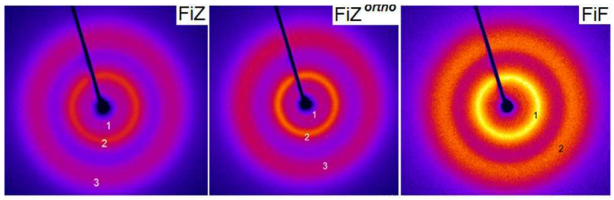


**Figure 4**. XRD patterns obtained from air-dried peptide stalks.

The data thus suggests that the assembly is attributed to interfacial coiled-coil interactions promoted by tryptophans.[12,13] However, to infer the extent and selectivity of these interactions, orthogonal constructs, FiZ$^{ortho}$ and FiB$^{ortho}$, had to be probed under the same conditions. In these peptides the same isopeptide bond disrupts the backbone continuity of $C_\alpha$ atoms directly affecting peptide folding. Given that three heptads used in each domain constitute a minimum requirement to yield stable coiled coils,[27] the peptides were still expected to fold, which was indeed observed (Figures 2A and S3). Yet, the lack of tryptophans, and hence potentially stabilizing interfacial contacts, for FiB$^{ortho}$ coiled coils along with their highly polar surfaces compounded by an anionic charge of the isopeptide glutamate should disfavour fibre formation. Conversely, FiZ$^{ortho}$ has two tryptophans in the original FiZ positions, which may support a more open packing of coiled coils leading to smaller and low density filaments. In accord with these assertions, TEM revealed scarce filamentous bundles of 15 nm in diameter for FiZ$^{ortho}$, with no assemblies observed for FiB$^{ortho}$ (Figure 3B). CD spectra for the same preparations exhibited $\Theta_{222}/\Theta_{208}$ ratios ≈ 1 suggesting the lack of lateral association for both peptides (Figure 2A). Unlike FiB$^{ortho}$, however, FiZ$^{ortho}$ folded cooperatively with a clear two-state transition upon melting (Figure S1). Similarly, SAXS and XRD signals could not be obtained for FiB$^{ortho}$ preparations at any concentrations used (0.1-3 mM). By contrast, SAXS for FiZ$^{ortho}$ gave two distinct radii of 1.2 ± 0.2 nm and 8 ± 5 nm, consistent with the diameters of individual coiled coils and the TEM-measured bundles, respectively (Figure 2B). Characteristic d-spacings at 9.6 and 4.4 Å in XRD patterns were similar to those obtained for FiZ indicating the same type of packing (Figure S2). An additional reflection at 18.6 Å was apparent and is important in two regards (Figures 4 and S2). Firstly, this spacing is right in between the corresponding spacings of FiZ (17.3 Å) and T2 (26.4 Å); and, secondly, it matches closely the size of 3D hexagonal lattices for axially packed coiled-coil staggers (18.2 Å).[6] This implies that though the isopeptide linkage disrupts super-helix contiguity in assembled coiled coils, the disruption occurs at regular pitch intervals allowing the staggers to propagate and interdigitate via tryptophan contacts. In marked contrast, FiB$^{ortho}$, which is the same sequence but lacking tryptophan residues, does not fold cooperatively or assemble (Figure S2). It is not unreasonable therefore to conclude that orthogonal breaks in FiZ disrupt the translation of the super-helix pitch in coiled-coil filaments and inhibit the assembly, while interfacial tryptophans provide sufficiently strong contacts to interlock coiled coils thereby outcompeting the disruption effect. Consequently, the tight packing characteristic of FiZ is loosened in FiZ$^{ortho}$ resulting in an increased spacing between packed coiled coils.

## Conclusions

In summary, we have introduced a physical rationale for engineering protein filamentous structures under morphological control. Protein filaments are major building blocks in naturally occurring systems that underpin an expanding variety of applications.[8] Regardless of their origin, use and function all filamentous materials rely on the same process of protein fibrillogenesis. The process produce highly uniform and regular structures including cytoskeleton microtubules or collagen fibres.[28,29] However, synthetic systems lack these characteristics and require additional constraints to control assembly from the molecule up.[30,31] Arguably, the best way to achieve this is by adopting tertiary elements characteristic of other folding motifs. Tryptophan residues provide a unique means in this case thanks to the tendency of indole rings to inter-lock.[12,13] Found in a handful of autonomously folded systems, such interlocking effects demand the precise positioning of tryptophan residues in peptide sequences. By applying these criteria in a coiled-coil folding motif we have set a regular pattern of interfacial interactions which enabled morphological control over filamentous assembly.[32,33] Notably, we have demonstrated, with an angstrom precision, traceable correlations between the precise positioning of tryptophan residues at the primary and secondary structure levels and the extent of ultrastructural packing in self-assembled filaments. We have experimentally attributed these correlations to the strength of tryptophan-regulated inter-coiled-coil interactions. The described rationale is applicable to other self-assembling systems and morphologies offering a promising strategy for engineering advanced physico-chemical systems and materials.

Physical Chemistry Chemical Physics Accepted Manuscript



This journal is © The Royal Society of Chemistry 20xx

Please do not adjust margins

## Experimental

**Peptide synthesis**: peptides were assembled on a Liberty-1 (CEM Corp.) using Fmoc-Gln(Trt)-Wang resin, standard solid phase Fmoc/tBu protocols and HBTU/DIPEA as coupling reagents. Following synthesis completion the peptides were cleaved from the resin by TFA:TIS:$H_2O$ – 95:2.5:2.5%, and purified by semi-preparative RP-HPLC on a JASCO HPLC system (model PU-980; Tokyo, Japan). Peptide purity and identity were confirmed by analytical HPLC and MALDI-ToF mass spectrometry (Bruker Daltonics) with 2,5-dihydroxybenzoic acid as a matrix.

MS $[M+H]^+$: FiZ – m/z 4716.7 (calc.), 4719.9 (found); FiF – m/z 4656.9 (calc.), 4656.3 (found); $FiZ^{ortho}$ – m/z 4659.8 (calc.), 4663.3 (found); $FiB^{ortho}$ – m/z 4543.4 (calc.), 4545.3 (found).

**High performance liquid chromatography**: analytical and semi-preparative gradient HPLC was performed on a Jasco HPLC system using a Grace C8 analytical (5 µm, 4.6 mm i.d. x 250 mm) and semi-preparative (5 µm, 10 mm i.d. x 250 mm) columns with 10-70% gradient of B (A: 95% $CH_3CN$, 5% $H_2O$, 0.1% TFA; B: 95% $CH_3CN$, 5% $H_2O$, 0.1% TFA) over 30 minutes at 1 mL/min and 4.7 mL/min flow rates, respectively, with detection at 214, 240 and 280 nm.

**Filamentous assembly and visualization by TEM**: peptide samples (300 µL, 100 µM) were incubated overnight in filtered (0.22 µm) 10 mM MOPS, pH 7.4 at 20°C. After incubation, a peptide aliquot (25 µL) was applied to a formvar/carbon coated copper/palladium support grids subjected to plasma glow discharge. After 5 minutes excess solution was blotted away, the sample was stained with 2% phosphotungstic acid and then examined using a Phillips BioTwin transmission electron microscope at the accelerating voltage of 80 kV.

**Circular dichroism (CD) spectroscopy**: CD spectra were obtained using a Chirascan Plus spectropolarimeter (Applied Photophysics Ltd.) equipped with a Peltier temperature controller. All measurements were taken in millidegrees for 100 µm peptide in 10 mM MOPS at pH 7.4 using 1 nm step, 1 nm bandwidth, 1 second time/point and 4 acquisitions in a quartz cuvette with 0.05 cm path length. A solvent baseline was recorded at a proximal time using the same experimental parameters. The four acquisitions were averaged and after baseline subtraction and normalisation for the concentration of peptide bonds the spectra were converted to mean residue ellipticities (MRE) (deg $cm^2$ $dmol^{-1}$ $res^{-1}$). CD spectra at variable temperature were recorded every 1°C from 20 to 90°C with 180 seconds equilibration time for each temperature point. Thermal denaturation curves were obtained by plotting the MRE at 222 nm as a function of temperature.

**Fourier-transform infrared (FT-IR) spectroscopy**: All FTIR spectra were collected using a Tensor-37 series FTIR spectrophotometer with a BioATR II unit (Bruker Optics, UK) as the sampling platform with a photovoltaic MCT detector and a Bruker Optics workstation, which was equipped with OPUS software. Aqueous samples of very low volume (15 µl, 100 µM) were placed in a circular sampling area of radius 2 mm with a path length of 6 µm. This multi-reflection ATR accessory is based on a dual crystal technology, which has an upper silicon crystal and a hemispherical zinc selenide (ZnSe) lower crystal that does not come into contact with the sample. The temperature of the sample was maintained at 20°C by means of flow connectors to a circulating water bath. This accessory was purged continuously throughout the experiment with dry nitrogen via telescopic inserts that seals the optical path inside the spectrometer sample compartment. All FTIR spectra were collected between 4000 and 850 cm-1 with resolution 4 cm-1, scanner velocity 20 kHz, 128 scans, phase resolution 32 and zero filling factor 4.

**Small angle X-ray scattering (SAXS)**: The SAXS experiments were carried out on the BioSAXS BM29 beamline at the ESRF (Grenoble, France). Solutions were loaded into PCR tubes in an automated sample changer kept at 20 °C. Around 50 µL from solutions were injected into a 1 mm quartz capillary and successive frames of 0.2 s each were registered during flow to avoid radiation damage. Data were recorded using a Pilatus 1M detector, positioned at sample-to-detector distance of 2,864 mm. The X-ray wavelength was $\lambda$ = 0.99 Å and reduction to 1-D intensity curves was performed by radial integration using the beamline software. This configuration provided high-resolution data in the range 0.051 $nm^{-1} \leq q \leq 4.97$ $nm^{-1}$ (where $q = 4\pi/\lambda \times sin\theta$, with $2\theta$ the scattering angle).

**SAXS data modeling**: The SAXS intensity from a system of disordered particles is dominated by the particle form factor. In our model, the form factor was fitted to a model for a long cylinder using the software SAS fit.[21] Briefly, this model assumes a cylinder radius R and a cylinder length L. We used a Gaussian distribution of R, with associated degrees of polydispersity $\Delta_R$. The background was fitted according to the Porod law $C_1+(C_2/q^{C3})$.[23] The length of the cylinder was fixed to $10^3$ Å for all the fits and behaved as a scale factor as R>>L in the form factor. The fitting parameters of the model are R, $\Delta_R$, $C_1$, $C_2$ and $C_3$.

**X-ray diffraction (XRD)**: X-ray diffraction specimens were prepared by suspending a drop of the peptide solutions between the ends of wax-coated capillaries and allowing them to dry. Using this method, FiF and T2 provided ~1 mm long peptide stalks while FiZ and $FiZ^{ortho}$ did not provide stalks visible by the naked eye. Instead, FiZ and $FiZ^{ortho}$ peptide solutions were dried on the wax head forming a protuberance that could be examined by XRD. All XRD patterns were compared versus the XRD of the wax heads supporting the samples. FiZ, FiF and $FiZ^{ortho}$ XRD specimens were mounted vertically onto the four axis goniometer of a RAXIS IV++ X-ray diffractometer (Rigaku) equipped with a rotating anode generator. The XRD data was collected using a Saturn 992 CCD camera. T2 XRD specimen was measured using synchrotron radiation ($\lambda$ = 0.6889 Å) at the I19 beamline of the Diamond Light Source (Didcot, UK). The specimen was mounted on the goniometer of a 4-circle Kappa goniometer. The XRD data was collected using a Saturn 724 CCD camera and a data acquisition software provided by Rigaku (CrystalClear). XRD data (rings) for samples with no positional ratio between reflections correspond to average distances between objects. The average distance is the spacing calculated from the position of the ring: spacing equals d = 2 x 3.14/q, where q is scattering vector for the position of the ring.

## Acknowledgements

We thank Bill Cowley and David Everest from Animal Health and Veterinary Laboratory Agency (AHVLA) for their help with

Physical Chemistry Chemical Physics Accepted Manuscript

TEM. We acknowledge Dr. Barbara Calisto at BM29 (ESRF, Grenoble, Project Number MX 1620) and Sarah Barnett for help with XRD measurement at beamline I19 (Diamond Light Source, Project Number MT11048), and Ian Hamley for access to the XRD instrument.

1 G. M. Whitesides, B. Grzybowski, *Science*, 2002, **295**, 2418.
2 E. De Santis, M. G. Ryadnov, *Chem. Soc. Rev*, 2015, doi: 10.1039/c5cs00470e.
3 H. Huebsch, D. J. Mooney, *Nature*, 2009, **462**, 426.
4 E. Gazit, *Chem Soc Rev*, 2007, **36**, 1263.
5 N. Stephanopoulos, J. H. Ortony, S. J. Stupp, *Acta Mater*, 2013, **61**, 912.
6 D. Papapostolou, A. M. Smith, E. D. T. Atkins, S. J. Oliver, M. G. Ryadnov, L. C. Serpell, D. N. Woolfson, *Proc. Natl. Acad. Sci. USA*, 2007, **104**, 10853.
7 Z. Xi, Y. Gao, G. Sirinakis, H. Guo, Y. Zhang, *Proc. Natl. Acad. Sci. USA*, 2012, **109**, 5711.
8 D. N. Woolfson, M. G. Ryadnov, *Curr. Opinion Chem. Biol.*, 2006, **10**, 559.
9 M. G. Ryadnov, A. Bella, S. Timson, D. N. Woolfson, *J. Am. Chem. Soc*, 2009, **131**, 13240.
10 E. De Santis, N. Faruqui, J. Noble, M. G. Ryadnov, *Nanoscale*, 2014, **6**, 11425.
11 B. Apostolovic, M. Danial, H. A. Klok, *Chem. Soc. Rev.* 2010, **39**, 3541.
12 A. G. Cochran, N. J. Skelton, M. A. Starovasnik, *Proc. Natl. Acad. Sci. USA*, 2001, **98**, 5578.
13 J. Liu, W. Yong, Y. Deng, N. R. Kallenbach, M. Lu, *Proc. Natl Acad. Sci. USA*, 2004, **101**, 16156.
14 A. Bella, M. Shaw, S. Ray, M. G. Ryadnov, *Sci. Rep.*, 2014, **4**, 7529. doi: 10.1038/srep07529.
15 P. B. Harbury, T. Zhang, P. S. Kim, T. Alber, *Science*, 1993, **262**, 1401.
16 B. Ciani, S. Bjelic, S. Honnappa, H. Jawhari, R. Jaussi, A. Payapilly, T. Jowitt, M. O. Steinmetz, R. A. Kammerer, *Proc. Natl Acad. Sci. USA*. 2010, **107**, 19850.
17 M. G. Ryadnov, D. N. Woolfson, *J. Am. Chem. Soc.*, 2005, **127**, 12407.
18 A. N. Lupas, M. Gruber, *Adv. Protein Chem.*, 2005, **70**, 37.
19 D. E. Wagner, C. L. Phillips, W. M. Ali, G. E. Nybakken, E. D. Crawford, A. D. Schwab, W. F. Smith, R. Fairman, *Proc. Natl. Acad. Sci. USA*, 2005, **102**, 12656.
20 J. D. Morrisett, R. L. Jackson, A. M. Gotto, *Biochim. Biophys. Acta*, 1977, **472**, 93.
21 T. M. Cooper, R. W. Woody, *Biopolymers* 1990, **30**, 657.
22 A. Chakrabartty, T. Kortemme, S. Padmanabhan, R. L. Baldwin, *Biochemistry*, 1993, **32**, 5560.
23 J. Kohlbrecher, I. Bressler, 2013 Software package sasfit for fitting small-angle scattering curves https://kur.web.psi.ch/sans1/SANSSoft/sasfit.html.
24 A. Guinier, G. Fournet, Small-Angle Scattering of X-rays, 1955, John Willey & Sons, Inc., New York.
25 E. K. O'Shea, J. D. Klemm, P. S. Kim, T. Alber, *Science* 1991, **254**, 539.
26 E. F. Banwell, E. S. Abelardo, D. J. Adams, M. A. Birchall, A. Corrigan, A. M. Donald, M. Kirkland, L. C. Serpell, M. F. Butler, D. N. Woolfson, *Nat. Mater.*, 2009, **8**, 596.
27 J. Su, R. S. Hodges, C. M. Kay, *Biochemistry* 1994, **33**, 15501.
28 S. Köster, D. A. Weitz, R. D. Goldman, U. Aebi, H. Herrmann, *Curr. Opin. Cell Biol.* 2015, **32**, 82.
29 K. E. Kadler, A. Hill, E. G. Canty-Laird, *Curr. Opin. Cell Biol*, 2008, **20**, 495.
30 K. Pagel, S. C. Wagner, K. Samedov, H. von Berlepsch, C. Böttcher, B. Koksch, *J. Am. Chem. Soc.* 2006, **128**, 2196.
31 A. Bella, S. Ray, M. Shaw, M. G. Ryadnov, *Angew. Chem. Int. Ed.* 2012, **51**, 428.
32 C. Xu R. Liu, A. K. Mehta, R. C. Guerrero-Ferreira, E. R. Wright, S. Dunin-Horkawicz, K. Morris, L. C. Serpell, X. Zuo, J. S. Wall, V. P. Conticello. *J Am Chem. Soc.*, 2013, **135**, 15565.
33 H. Dong, S. E. Paramonov, J. D. Hartgerink, *J Am Chem. Soc*. 2008, **130**, 13691.

Physical Chemistry Chemical Physics Accepted Manuscript



This journal is © The Royal Society of Chemistry 20xx

Please do not adjust margins